Moroccan Journal of Chemistry
ISSN: 2351-812X
http://revues.imist.ma/?journal=morjchem&page=login
Bettach & al / Mor. J. Chem. 7 N°2 (2019) 236-241

Structure refinement, EPR, Specific magnetic heat and magnetic properties of $ZnMnP_2O_7$ diphosphate

Mohammed Bettach[1*], Yassine Ennaciri[1], Mustapha Touaiher[2] and Khalil Benkhouja[2]

[1] *LPCM, UCD, Faculty of Sciences, Department of Chemistry, BP 20, El Jadida, Morooco.*
[2] *LCCA, UCD, Faculty of Sciences, Department of Chemistry, BP 20, El Jadida, Morooco.*

** Corresponding author:*
bettachmohammed@yahoo.fr
Received 25 Dec 2018,
Revised 05 Feb 2019,
Accepted 22 May 2019

Abstract

The structure of the diphosphate $ZnMnP_2O_7$ is determined on powder by the Rietveld method. It is of monoclinic symmetry C2/m. The cell parameters are: a = 6.6141(3) Å, b = 8.4366 (3) Å, c = 4.5305(2) Å and β= 103.948(2) °. The structural framework is built by MO_6 octahedron planes where M is a mixed site statistically occupied by Zn^{2+} and Mn^{2+} ions. These planes are parallel to the crystallographic plane (001) and are linked together by sheets of $P_2O_7^{4-}$ groups. The value of the paramagnetic temperature Θp is -4 K, which proves that the interactions are antiferromagnetic . The magnetic specific heat of this compound has a symmetric maximum at T = 5.3 K less acute compared to that of $Mn_2P_2O_7$ of isotypic structure which is of λ type. This behavior change can be explained by the interruption of the three-dimensional interactions between Mn^{2+} ions which become limited to 2D order when 50% of these ions are replaced by Zn^{2+} ions.

Keywords: Diphosphate, Zinc, Manganese, Structure, Magnetism, EPR, specific heat.

1. Introduction

Metal polyphosphates show a great variety of compositions, crystal structures, and properties. Nowadays, they have become an important constituent class of compounds for exploring new functional materials. Taking into a count their thermal and phase stability, they are of a great importance for application in sensors, solid-state laser materials, piezoelectric, luminophor, ceramics, catalysis, adsorption, ionic conductors, and magnetic materials [1-3]. The crystallochemical study carried out on the $Zn_xMn_{2-x}P_2O_7$ system ($0 \leq x \leq 2$) [4] shows that $ZnMnP_2O_7$ diphosphate is isotypic to $Mn_2P_2O_7$ (or β-$Zn_2P_2O_7$) of C2/m symmetry [2, 3]. Also, the differential thermal analysis measurements reveal that this compound has a single allotropic variety. This allowed us to refine its structure on powder using the Rietveld method [4]. In reference to our works when we tried to reduce the dimensionality in the mixed diphosphates $Zn_xM_{2-x}P_2O_7$ ($0 \leq x \leq 2$) (M=Mn, Co, Ni, Cu) by Zn^{2+} and in $LiNi_{1.5}P_2O_7$ by Li^+ [4, 8-11], we present in this work the magneto-structural correlation in $ZnMnP_2O_7$. Measures of magnetic susceptibility, magnetic specific heat and electron paramagnetic resonance were realized on the diphosphate $ZnMnP_2O_7$ to correlate these properties to its crystalline structure. The values of Landé factor g are isotropic and confirm that the sites occupied by Mn^{2+} are regular. The evolution of the magnetic specific heat indicates that 3d order is interrupted. The magnetic interactions are antiferromagnetic.

2. Methodology

2.1. Synthesis

$ZnMnP_2O_7$ diphosphate is prepared in powder by the ceramic method from the reagents $ZnCO_3$, $MnCO_3$ and $(NH_4)_2HPO_4$, these reagents taken in stoichiometric proportions are finely ground in an agate mortar. Afterwards, the mixture is placed in a silica crucible, kept in air at 120 °C for 15 hours and gradually brought to 500 °C in order to avoid a sudden decomposition of carbonates or ammonium hydrogenophosphate. Once the decomposition is complete, the mixture is well grounded and treated at 900 ° C for 24 hours. Finally, the powder is quenched in the air

.

2.2. Characterization

X Ray Diffraction: powder diffractogram of $ZnMnP_2O_7$ compound is recorded at room temperature using a Siemens D5000 diffractometer equipped with a copper anticathode and a graphite monochromator. The intensities are scanned according to the Bragg-Brenato geometry $\theta/2\theta$. The X-ray diffraction data, used to refine the structure by the Rietveld method, are collected between 10 and 125 ° in 2θ with a step of 0.03 ° and a counting time of 22 s.

Electronic Paramagnetic Resonance: The electronic paramagnetic resonance measurements are performed at 4K, 77K and 298K using a BRUKER device at a frequency of 9.5 GHz. Measurement of Magnetic Susceptibility: The measurement of magnetic susceptibility was carried out on a vibrating magnetometer "DMS8" using the Faraday method in the temperature range 4 to 300 K and under an applied field of 14 KOe. Magnetic susceptibility values are corrected from diamagnetic and Van Vleck contributions. Magnetic Specific Heat Measurement: The measurement of the specific heat Cp was accomplished using a calorimeter equipped with an adiabatic screen developed by Kuentzler (Institute of Physics, IPCMS, Strasbourg - France).

3. Results and discussion

3.1. Structure refinement

The analysis of $ZnMnP_2O_7$ powder diffractogram by the Rietveld method is realized using the PC version of the GSAS software [12]. The initial model used to refine the structure is the diphosphate $Mn_2P_2O_7$ of monoclinic symmetry C2/m. The pseudo-Voigt function including an asymmetry correction is chosen for a better modeling of the diffractogram peaks profile [13, 14]. The convergence is completed after refinement of the scale factor and the continuous background, the cell parameters, the zero shift, the parameters of the profile and finally the atomic positions and the isotropic thermal agitation factors.

The crystallographic data of $ZnMnP_2O_7$ are summarized in Table 1.The R_{wp}, R_p and R_F reliability factors are used to estimate the agreement between the model and the experiment. R_p and R_{wp} characterize the agreement between calculated and observed

diffractograms. R_F describes the agreement between the structure and the intensities observed. The value of R_F (0.061) shows a good agreement between the model and the experiment. Figure 1 represents the diffractograms calculated, observed and their difference as well as the positions of the peaks for the diffractogram recorded at ambient temperature.

Table 1. Crystallographic data of $ZnMnP_2O_7$

Compound	**$ZnMnP_2O_7$**
Système	Monoclinique
Groupe d'espace	C2/m
Z	2
M(g/mol)	294,25
a (Å)	6,6141(3)
b (Å)	8,4366(3)
c (Å)	4,5305(2)
β(°)	103,948(2)
V ($Å^3$)	245,35(2)
ρ ($g.cm^{-3}$)	3,983
R_{wp} (%)	14,9
R_p (%)	11,4
R_F (%)	6,1

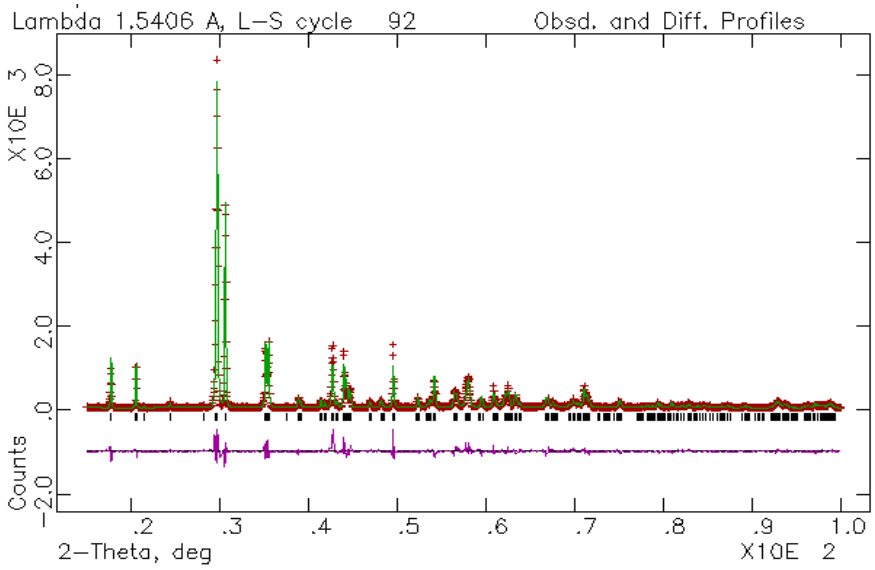

Figure 1. Diffractograms calculated, observed and difference of $ZnMnP_2O_7$ diphosphate.

Table 2. Atomic positions and isotropic thermal agitation coefficients in $ZnMnP_2O_7$ structure

Atome	x	y	z	$U_{iso}(Å^2)$
M	0,0000	0,3096(3)	0,5000	0,0188(8)
P	0,2131(7)	0,0000	-0,0921(9)	0,017(1)
O1	0,0000	0,0000	0,0000	0,056(6)
O2	0,374(1)	0,0000	0,210(2)	0,0043(3)
O3	0,2280(8)	0,1484(6)	0,727(1)	0,010(2)

The coordinates of the atomic positions and the isotropic thermal agitation coefficients are grouped together in Table 2. The interatomic distances and inter-bond angles in the PO_4 and MO_6 coordination polyhedra are presented in Table 3. The notation M designates the mixed site (Zn, Mn).

Table 3: principal interatomic distances (Å) and angles (°) between bonds in $ZnMnP_2O_7$

P_2O_7				MO_6			
P–O1	1,563(5)	O1–P–O2	103,9(4)	M–O2^{iii}	2,115(5)	O2^{iii}–M–O2^{iv}	81,3(4)
P–O2	1,515(9)	O1–P–O3^{i}	109,0(3)	M–O2^{iv}	2,115(5)	O2 ^{iii} –M–O3	157,3(2)
P–O3^{i}	1,514(5)	O1–P–O3^{ii}	109,0(3)	M–O3	2,107(5)	O2 ^{iii} –M–O3^{v}	93,3(2)
P–O3^{ii}	1,514(5)	O2–P–O3^{i}	111,5(3)	M–O3^{v}	2,107(5)	O2 ^{iii} –M–O3^{vi}	80,8(2)
		O2–P–O3^{ii}	111,5(3)	M–O3^{vi}	2,303(5)	O2 ^{iii} –M–O3^{vii}	85,8(2)
< P–O>	1,527	O3i–P–O3^{ii}	111,6(5)	M–O3^{vii}	2,303(5)	O2 ^{iv}–M–O3	93,3(2)
P-O1-P	180					O2^{iv}–M–O3^{v}	157,3(2)
		<O–P1–O>	109,4	< M–O>	2,175	O2^{iv}–M–O3^{vi}	85,8(2)
						O2^{iv}–M–O3^{vii}	80,8(2)
						O3–M–O3^{v}	99,4(3)
						O3–M–O3^{vi}	76,8(2)
						O3–M–O3^{vii}	115,2(2)
						O3^{v}–M–O3^{vi}	115,2(2)
						O3^{v}–M–O3^{vii}	76,8(2)
						O3^{vi}–M–O3^{vii}	162,4(3)

Symmetry Code: (i) (x, y, z-1) ; (ii) (x, -y, z-1) ; (iii) (x-1/2, y+1/2, z) ; (iv) (1/2-x, y+1/2, 1-z) ; (v) (-x, y, 1-z) ; (vi) (1/2-x, 1/2-y, 1-z) ; (vii) (x-1/2, 1/2-y, z).

3.2. Description of the structure and discussion

The projection of the $ZnMnP_2O_7$ structure on the (010) plane is shown in figure 2. This structure is reminiscent of the thortveitite $Sc_2Si_2O_7$ [15]. It is formed by MO_6 octahedron planes where M is a mixed site occupied statistically by the Zn^{2+} and Mn^{2+} ions with a ratio 50/50.These planes are parallel to the crystallographic plane (001) and are linked to each other by the planes of P_2O_7 groups. Figure 3 illustrates the projection of $ZnMnP_2O_7$ structure on the (001) plane. We observe that each octahedron is linked to three other neighbors and shares an edge with each one. The sequence of these octahedra can be described by planes of honeycomb hexagons in which the P_2O_7 groups are stacked. The P_2O_7 groups have a staggered conformation, the POP angle is linear, the bridge PO distance is 1.563 Å and the average distance of the terminal PO bonds is 1.514 Å, the OPO angles value varie between 103.9° and 111.6°. These values are close to those obtained for $Mn_2P_2O_7$. The average value of the equatorial M-O distances is 2.11 Å and that of the axial distances is 2.30 Å. The average values of the equatorial and axial distances are respectively 2.03 Å and 2.27 Å for β-$Zn_2P_2O_7$ and 2.15 Å and 2.32 Å in the case of $Mn_2P_2O_7$. We note that the size and the deformation of the MO_6 octahedra is intermediate between those of the ZnO_6 octahedra in β-$Zn_2P_2O_7$ and those of the MnO_6 octahedra in $Mn_2P_2O_7$. We take into account that the compound $ZnMnP_2O_7$ is isotypic with β-$Zn_2P_2O_7$ and $Mn_2P_2O_7$ and that the ionic radii of Zn^{2+} and Mn^{2+} are respectively 0.74 Å and 0.80 Å. This diphosphate $ZnMnP_2O_7$ is related to the mixed diphosphates of two 3d transition elements that crystallize in the thortveitite structural type with mixed occupation of octahedral sites by metal ions such as $CuZnP_2O_7$ [16], $Ni_{1.18}Mn_{0.8}P_2O_7$ and $Ni_{0.42}Mn_{1.58}P_2O_7$ [17] and $Cu_{0.92}Mn_{1.08}P_2O_7$ [18]

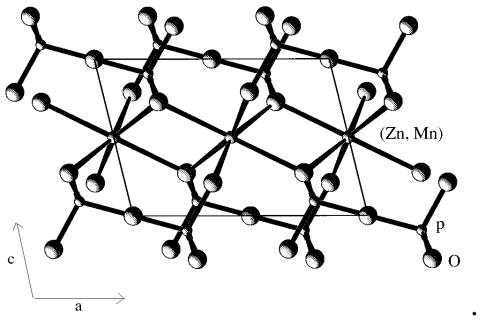

Figure 2. Projection of $ZnMnP_2O_7$ structure on the crystallographic plane (010).

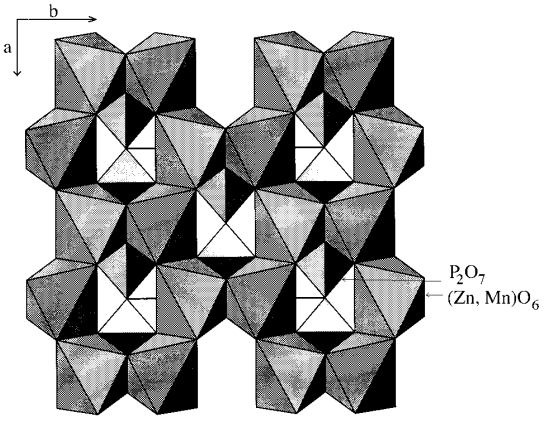

Figure 3. Projection of $ZnMnP_2O_7$ structure on the crystallographic plane (001).

3.3. Magnetic properties

3.3.1. Electron Paramagnetic Resonance

Figure 4 represents the EPR spectra of the $ZnMnP_2O_7$ diphosphate at temperatures of 4 K, 77 K and 298 K. They are isotropic. The value of g (Landé factor) is almost constant and is 2.02 at different temperatures. This value does not differ much from that obtained on single crystals of β-$Mg_2P_2O_7$ and β-$Zn_2P_2O_7$ doped with Mn^{2+} [19-21] and which are isotypic with the pyrophosphate $ZnMnP_2O_7$. In these three compounds, the Mn^{2+} ion occupies octahedral sites. The ground state $^6A_1$ is well isolated from other higher energy levels. The spin-orbit coupling is zero and the zero-field splitting is very weak. This confirms the isotropic value of g obtained for the compound $ZnMnP_2O_7$.

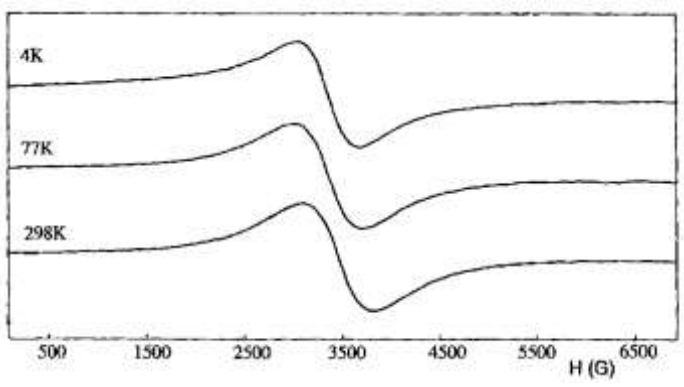

Figure 4. EPR spectra of $ZnMnP_2O_7$ diphosphate.

3.3.2. Magnetic susceptibility

The simple pyrophosphate $Mn_2P_2O_7$ exhibits an antiferromagnetic behavior at low temperature. The experimental values of T_N (Neel temperature) and Θp (Curie paramagnetic temperature) taken from the thermal variation curve of the inverse of the magnetic susceptibility $\chi^{-1} = f(T)$ are respectively 13K and -11K. They are very close to those given in the literature [22, 23]. The magnetic structure of $Mn_2P_2O_7$ proposed by M. F. Collins et al. [24], shows that the interactions in the sheets of Mn^{2+} ions parallel to the plane (001) are antiferromagnetic, whereas those intersheets are ferromagnetic; they are weak because the sheets of Mn^{2+} ions are separated by planes of $P_2O_7^{4-}$groups, and the distance between two successive sheets is large and is equal to the parameter c (c = 4.546 Å). The coupling between sheets is done by super-exchange as follows: Mn-O-P-O-Mn. The global interactions in $Mn_2P_2O_7$ are antiferromagnetic. The thermal variation curves of the magnetic susceptibility and the product χ.T for $ZnMnP_2O_7$ are represented in figure 5. We remark that the acute maximum of χ characteristic of a three-dimensional order observed at 11 K for $Mn_2P_2O_7$, is displaced to about 7 K for $ZnMnP_2O_7$ diphosphate. Indeed, the increase of the zinc rate causes a shift of the maximum towards the low temperatures. This is explained by a magnetic dilution that weakens the exchange interactions between paramagnetic ions. The curve $\chi^{-1} = f(T)$ of $ZnMnP_2O_7$ (figure 6) follows a Curie-Weiss law above 7 K (Θp = -4K). The value of the Curie constant is 4.1 uem.K / mol, it is close to that calculated for single spin interactions and confirms the presence of one Mn^{2+} ion per molecule of $ZnMnP_2O_7$. The product χ.T remains constant in a wide range then decreases rapidly and tends to zero for the lowest temperatures. This behavior characteristic of antiferromagnetic order can be explained by the antiparallel coupling of Mn^{2+} ions inside the sheets, which engenders compensation between magnetic moments.

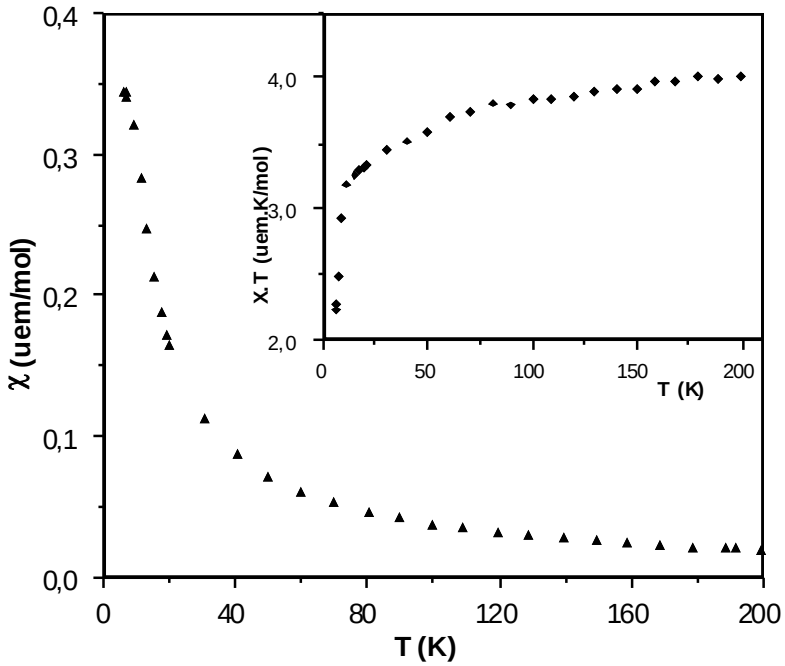

Figure 5. Thermal variation of magnetic susceptibility and χ.T product of $ZnMnP_2O_7$.

The graphical representation of the line $Cp.T^2 = f(T^5)$ for the highest temperatures where the contribution of the network is predominant (T> 17K) permit to calculate the parameter a ($a = 5.10^{-4}$) and consequently to deduce this contribution knowing that $Cp(net) = aT^3$. We note that the specific magnetic heat has a maximum at T ~ 5.3 K, which is symmetrical and a little wide. This behavior can be interpreted by a Schottky anomaly due to the weak zero-field splitting of the ground state $^6A_1$ of Mn^{2+} ions. In addition the non-acute maximum can be explained by the interruption of the three-

dimensional order in $Mn_2P_2O_7$ already reported by M. F. Colins and al. [20] by substituting 50% of the Mn^{2+} ions with Zn^{2+} ions. The specific heat of the compound $Ni_{0,2}Mn_{1,8}P_2O_7$ isostructural to $Mn_2P_2O_7$ reported by K. Benkhouja and al [25] presents an acute maximum of λ type characteristic of a three-dimensional order that is not observed for $ZnMnP_2O_7$; which confirms that the interactions were limited to 2D order in the cationic planes while the interactions between neighboring planes are weakened

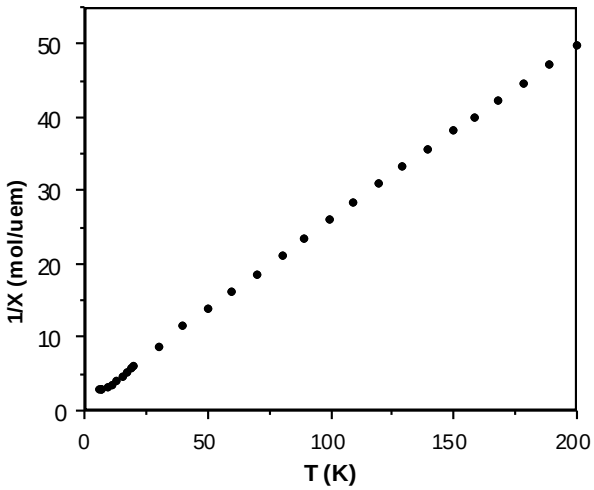

Figure 6. Thermal variation of the inverse of magnetic susceptibility of $ZnMnP_2O_7$.

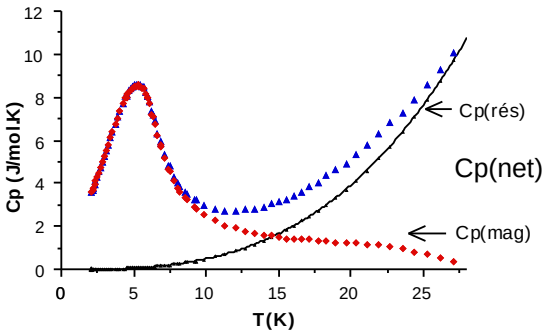

Figure 7. Thermal variation of the specific heat of $ZnMnP_2O_7$ diphosphate.

4. Conclusion

The diphosphate $ZnMnP_2O_7$ is prepared by the ceramic method. Its crystalline structure is refined on powder by the Rietveld method using the $Mn_2P_2O_7$ crystallographic data of isotypic structure at the beginning. It is of monoclinic symmetry C2/m. The Mn^{2+} and Zn^{2+} ions occupy statistically the octahedral sites. The $P_2O_7^{4-}$ groups have a staggered conformation of the thortveitite type. The interatomic distances have intermediate values between those of $Zn_2P_2O_7$ and $Mn_2P_2O_7$. The results of RPE show that g is constant and equal to 2.02 at different temperatures which assert that the Landé factor is isotropic. The evolution of the magnetic susceptibility of $ZnMnP_2O_7$ is characteristic of antiferromagnetic behavior. The magnetic specific heat has a slightly larger maximum compared to that of $Mn_2P_2O_7$ of λ type. This change is due to an interruption of the 3D order because of the substitution of paramagnetic ions Mn^{2+} by diamagnetic ions Zn^{2+}.

5. References

[1] Echabaane M. Rouis A. Bonnamour I.& Ben Ouada H., Mor. J. Chem.4 N°3 (2016) 849-853

[2] Sahraoui M. Abderrahmen A. Ben Ouada A. & Gharbi A. Mor. J. Chem.4 N°3 (2016) 651-660

[3] Mohamed Sikkander A. & Shawl Nasri N., Mor. J. Chem. 1 N°2 (2013) 47-54

[4] Bettach M., Benkouja K., Sadel A., Zahir M. & M. Drillon, Adv. Mat. Resh. 1 (1994) 543-552.

[5] Stefanidis T. & Nord A. G., Acta Cryst. C40(1984) 1995-1999.

[6] Calvo C., Can. J. Chem. 43,(1965), 1147.

[7] Rietveld. H. M. J. Appl. Crystallogr. 2(1969) 65-71.

[8] Rissouli K., Benkhouja K., Sadel A., Bettach M., Zahir M., Giorgi M.& Pierrot M., Acta Crys. C52 (1996) 2960-2963

[9] Rissouli K., Bettach M., Benkhouja K., Sadel A., Zahir M., Pierrot M., Derrory A. & Drillon M. Ann. Chim. Sci. Mat, 23, (1998) 103-l06

[10] Bettach M., Touaiher M.& K. Benkhouja, Mol. Cryst. Liq. Cryst. 627(2016) 118-124

[11] Bettach M., Benkhouja K., Zahir M., Rissouli K., Sadel A., Giorgi M. Pierrot& M., Acta Cryst. C54, (1998), 1059-1062.

[12] Larson A. C. & Dreele R. B., GSAS : Generalised structure analysis system ; Los Alamos National Laboratory : Los Alamos, NM, 1994.

[13] Thomson P., Cox D. E., J. B. Hasting, J. Appl. Crystallogr. 20 (1987) 79-83

[14] Finger L. W., Cox D. E., Jephcoat A. P., J. Appl. Crystallogr. 27 (1994) 892-900

[15] Cruickshank D. W. J., Lynton H. & Barclay G. A., Acta Cryst. 15 (1962) 491-498

[16] ElMaadi A., Boukhari A., Holt E. M. & Flandrois S., J. All. Comp., 205 (1994) 1241-1246

[17] Benkhouja K., Zahir M., Sadel A., Handizi A., Boukhari A., Holt E. M., Aride J. & Drillon M., Mat. Res. Bull. 30 (1995) 49-55

[18] Handizi A., Boukhari A., Holt E. M., Aride J., Belaiche M. & Drillon M., Europ. J. Sol. Stat. Inorg. Chem., 31 (1994) 123 -127

[19] Chambers J. C., Datars W. R. & Calvo C., J. Chem. Phys. 41(3) (1964) 806-813

[20] Calvo C., Leung J. S. & Datars W. R., J. Chem. Phys. 46(2) (1967) 796-803

[21] Gupta S. K., Kadam G. R. & Samui P., J. Mater. Res. 28 (2013) 3157-3163

[22] Fowlis D. C. & Stager C. V., Can. J. Phys. 47 (1969) 371-373

[23] Wung Ho Choh & Stager C. V., Can. J. Phys. 48 (1970) 521-530

[24] M. F. Collins, G. S. Gill et C. V. Stager, J. Phys. 49 (1971) 979-982

[25] K. Benkhouja Thesis, University of Chouaib Doukkali, El Jadida, Morocco (1994).